

Magnons in a two-dimensional transverse-field XXZ modelSatyaki Kar,¹ Keola Wierschem,² and Pinaki Sengupta²¹*Theoretical Physics Department, Indian Association for the Cultivation of Science, Jadavpur, Kolkata 700032, India*²*School of Physical and Mathematical Sciences, Nanyang Technological University, 21 Nanyang Link, Singapore 637371*

(Received 30 December 2016; revised manuscript received 18 June 2017; published 19 July 2017)

The XXZ model on a square lattice in the presence of a transverse magnetic field is studied within the spin-wave theory to investigate the resulting canted antiferromagnet. The small- and large-field regimes are probed separately both for easy-axis and easy-plane scenarios which reveal an unentangled factorized ground state at an intermediate value of the field. Goldstone modes are obtained for the field-free XY antiferromagnet as well as for the isotropic antiferromagnet with field up to its saturation value. Moreover, for an easy-plane anisotropy, we find that there exists a nonzero field, where magnon degeneracy appears as a result of restoration of a $U(1)$ sublattice symmetry and that, across that field, there occurs a magnon band crossing. For completeness, we then obtain the system phase diagram for $S = 1/2$ via large-scale quantum Monte Carlo simulations using the stochastic series expansion technique. Our numerical method is based on a quantization of spin along the direction of the applied magnetic field and does not suffer from a sign problem, unlike comparable algorithms based on a spin quantization along the axis of anisotropy. With this formalism, we are also able to obtain powder averages of the transverse and longitudinal magnetizations, which may be useful for understanding experimental measurements on polycrystalline samples.

DOI: [10.1103/PhysRevB.96.045126](https://doi.org/10.1103/PhysRevB.96.045126)**I. INTRODUCTION**

Quantum magnets have long served as the ideal framework for exploring novel quantum phases and phenomena in interacting many-body systems [1]. From a theoretical standpoint, the reduced Hilbert space renders the systems amenable to powerful analytic and computational techniques. Consequently, the interplay between competing interactions, crystal electric field effects, lattice geometry, and (in many cases) geometric frustration can be studied systematically in a well-controlled manner. At the same time, rapid advances in material synthesis and characterization techniques have resulted in a wide array of quantum magnets where many such novel quantum phases can be realized and investigated experimentally. Some examples include Bose-Einstein condensation of magnons [2], spin-liquid phases [3], valence bond solids [4,5], topologically nontrivial noncoplanar spin textures [6,7], and magnetization plateaus [8].

The XXZ model—and its straightforward generalizations—remain the standard paradigm for describing the vast majority of quantum magnets, making this family of Hamiltonians arguably the most intensively studied family of microscopic models of interacting many-body systems. The simple $SU(2)$ variant of the model, in conjunction with additional terms such as uniaxial anisotropies, on different lattice geometries yields a rich array of field-driven phases with unique functionalities. Since many of these novel states can be controllably realized in real quantum magnets by applying an appropriate external magnetic field, the behavior of the XXZ model and its multiple variants in an external field has been an active frontier of analytic and numerical investigation. As a prototypical example, the quasi-one-dimensional (quasi-1D) compound Cs_2CoCl_4 has been studied at length as a system that can realize an XXZ antiferromagnet under an applied transverse field [9–11]. To date, most of the studies have utilized a longitudinal magnetic field [12–14]. In contrast, the study of a transverse field

remains relatively less studied [15,16]. However, such an investigation is important from an experimental standpoint. Often, the chemical composition of spin compounds makes it very difficult to synthesize single crystals, and the experimental characterization has to rely on powder samples. This is particularly true for neutron-scattering studies (both elastic and inelastic)—possibly the most powerful experimental probes to identify different magnetic states. Neutron-scattering experiments require relatively large samples and, for materials where large single crystals are unachievable, one works with pellets of powder samples which are comprised of microscopic domains of single crystals with randomly oriented axes. When such a sample is placed in a magnetic field, each domain experiences a field in a different direction relative to its crystal axis and the measurements yield the average of fields along different directions. For a direct comparison of theoretical studies with such experiments, a detailed study of the effects of a transverse field on an XXZ model is important and can be combined with results for a longitudinal field to estimate (approximately) the powder average.

Aside from quantum magnets, the study of the XXZ model in a transverse field is important from a quantum-computational point of view as well [17]. While a longitudinal magnetic field renders the model exactly solvable in one dimension by the Bethe ansatz, integrability is lost in the presence of a transverse magnetic field [18]. Quantum correlations give rise to entanglement, and the ability to control the amount of entanglement in a system by using a noncommuting field may play an important role in quantum technology applications [19]. Furthermore, by tuning the transverse field in an XXZ model, it is possible to obtain an unentangled state [20]. This phenomenon of ground-state factorization indicates an entanglement phase transition which has no classical analog [21].

Though a transverse-field XXZ (TF-XXZ) model has been studied previously [15,16], a rigorous investigation of the sublattice structures as well as the magnon modes as a

function of the transverse field has been long due. In order to bridge that gap in the literature, in this paper we use spin-wave theory (SWT) to explore the evolution of the magnetic ground states and their low-lying excitations as the transverse field strength is gradually increased. Hamiltonian symmetries and their symmetry breakings, as well as the corresponding degeneracies and Goldstone excitations, are analyzed in detail. We also identify the special entanglement free point in the phase space that appears at the so-called factorizing field [17] $h = h_f$. Magnon modes are obtained in the resulting canted antiferromagnet (AFM) and magnetization along the field direction is observed. The analytical studies are complemented by large-scale quantum Monte Carlo (QMC) study using the stochastic series expansion technique in order to obtain the system phase diagram. The two-dimensional (2D) TF-XXZ model has been studied using the quantum Monte Carlo method before [16], and here our approach is essentially the same. In addition to identifying the different ground-state phases as the parameters are varied, we extract powder-averaged values for the magnetization (weighted averages over the longitudinal and transverse field components of the magnetization), which are useful for analyzing the results of experimental measurements on polycrystalline samples [22].

II. MODEL

We investigate the $S = 1/2$ XXZ model with both Ising and XY anisotropies in longitudinal as well as transverse external magnetic fields. A generic XYZ model in a magnetic field \vec{h} can be written as

$$\mathcal{H} = \sum_{(ij)} J_x S_i^x S_j^x + J_y S_i^y S_j^y + J_z S_i^z S_j^z - \sum_i \vec{h} \cdot \vec{S}_i, \quad (1)$$

where J_x, J_y, J_z denote the spin-exchange interactions along the x, y, z spin axes and are summed over nearest-neighbor pairs on the square lattice. From here, a TF-XXZ model may be derived by setting the spin-exchange interactions to $J_x = J_y = J_\perp$ with $J_z/J_\perp = \Delta$, and applying the transverse field along the x axis, $\vec{h} = h\hat{x}$. In zero field, the XXZ model is gapless for $-1 \leq \Delta \leq 1$ while it is gapped with an Ising anisotropy for $\Delta > 1$. Néel long-range order is observed in the gapped Ising-like phase, while the gapless XY-anisotropic regime also exhibits long-range Néel order but is instead characterized by the presence of Goldstone modes due to the breaking of a continuous U(1) symmetry.

The U(1) symmetry of the XXZ model is lost upon adding the transverse magnetic field. At zero magnetic field, there is no magnetization in the system and the quantization axis is decided by the exchange anisotropy parameter $J_z/J_\perp = \Delta$ yielding an easy-axis AFM for $\Delta > 1$ and an easy-plane AFM for $\Delta < 1$. The magnetic field turns on the magnetization in the system. With a transverse field along the x direction, the total spin along the exchange anisotropy direction becomes nonconserving away from the Heisenberg point $\Delta = 1$. A perpendicular antiferromagnetic order appears with spins canted towards the field direction. In other words, we obtain simultaneous spin alignment along the x direction and antiferromagnetic ordering in the z (for $\Delta > 1$) or y (for $\Delta < 1$) direction (see Fig. 1). The magnetization along the x direction (m_x) increases monotonically with magnetic field h until it

reaches the critical field $h = h_c$ where antiferromagnetic order is extinguished and spins align almost completely (for $\Delta \neq 1$) in the x direction, forming a (nearly) saturated paramagnetic phase. However, it needs an infinitely large field, away from the Heisenberg point, to ensure complete polarization along the field.

In addition to describing the quasi-one-dimensional magnet Cs_2CoCl_4 for fields applied along the b axis [9], the TF-XXZ model is also related to effective models for certain quantum magnets where an alternating g -tensor and/or Dzyaloshinskii-Moriya interaction can give rise to an effective staggered field [23]. Such an effective model has successfully been applied to the quasi-one-dimensional quantum magnet copper benzoate [23–25].

In this work, we focus on the case of a uniform magnetic field perpendicular to the axis of exchange anisotropy in a spin-1/2 XXZ model on the square lattice. The easy-axis version of this model was previously considered by Jensen *et al.* [15] using a Green's function approach. Their main conclusion was that for small fields, the reduction in spin fluctuations dominates over the spin canting, leading to an increase in the staggered magnetization m_s along the Ising axis, as well as to an increase in the Néel temperature T_N . At higher fields, of course, the trend reverses, until both m_s and T_N are zero at the critical field.

III. SPIN-WAVE THEORY

In order to develop the spin-wave analysis for the transverse-field XXZ model with magnetic field h along the x direction, we need to first identify how the quantization direction changes with h . An Ising anisotropy causes the spin quantizations in the two sublattices to be along $\pm z$ directions. But U(1) symmetry in the XY anisotropic case forbids any such preferences for quantization direction in the x - y plane. With infinitesimal h along x , however, the symmetry is broken and spin flop process results in the perpendicular $\pm y$ directions to stand out as the quantized axes (see Fig. 1). As h is increased, the sublattice magnetization starts canting towards the x direction until it becomes parallel to the x axis, though the maximal value of the spin is reached at an infinite value of

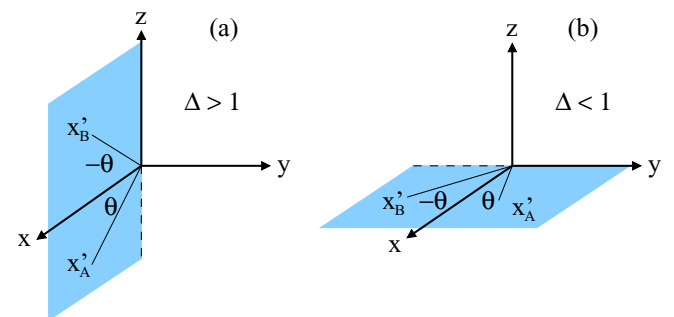


FIG. 1. Canting of the spin quantization axis in a transverse field directed along x . For nonzero field, the spins are canted parallel to the x' axes. The canting occurs (a) in the x - z plane (with $y' = y$) for $\Delta > 1$ and (b) in the x - y plane (with $z' = z$) for $\Delta < 1$. Here xyz denotes the original uncanted frame while $x'_{A(B)}$ refers to the transformed x axes in the A (B) sublattices of the canted frame.

h in the presence of exchange anisotropy. There exists a finite critical value of the field at which the spins align parallel to the field: this is marked by a sharp change in the slope of the m_x vs h curve with the magnetization close to its saturation value. Beyond this critical field, the magnetization increases slowly (due to decrease in quantum fluctuations) towards full polarization which is reached theoretically at an infinite field. At some nonzero $h = h_f$, a factorized ground state is obtained where entanglement becomes zero. In the case of an Ising (XY) anisotropy, we first perform a spin-coordinate rotation by an angle $\pm\theta$ about the spin- y (spin- z) axis in the A (\uparrow) and B (\downarrow) sublattices, respectively. Calling the canted new x directions the quantization directions, a ferromagnetic state is obtained in the transformed coordinates.

Within the linear spin-wave approximation in this rotated frame, the easy-plane XXZ Hamiltonian gets transformed to (for the remainder of this section we set J_\perp to unity and use it as our unit of measurement)

$$H = E_0(\theta) + \sum_{\langle ij \rangle} \left[\frac{h}{Z} (n_i + n_j) \cos \theta - \cos(2\theta) S(n_i + n_j) + \frac{\cos 2\theta - \Delta}{4} (a_i^\dagger b_j^\dagger + \text{H.c.}) + \frac{\cos 2\theta + \Delta}{4} (a_i^\dagger b_j + \text{H.c.}) + \frac{2h \sin \theta / Z - \sin 2\theta}{4} (a_i^\dagger - b_j^\dagger + \text{H.c.}) \right].$$

Here n_i (n_j) and a_i (b_j) are spin deviation and bosonic annihilation operators, respectively, at site i (j) within the \uparrow (\downarrow) sublattice and Z is the coordination number ($Z = 4$ in the 2D XXZ model). See Appendix A for details. Minimizing $E_0(\theta)$ identifies the state of quantization by selecting the reference angle θ_r with $\cos \theta_r = h/2ZS$. A Fourier transformation, from there on, leads to

$$H = E_0(\theta_r) + \sum_k \left[ZS(a_k^\dagger a_k + b_k^\dagger b_k) + ZS\gamma_k \left(\frac{\cos 2\theta_r + \Delta}{2} (a_k^\dagger b_k + \text{H.c.}) + \frac{\cos 2\theta_r - \Delta}{2} (a_k^\dagger b_{-k}^\dagger + \text{H.c.}) \right) \right] \quad (2)$$

with $\gamma_k = (\cos k_x + \cos k_y)/2$. We need to resort to a 4×4 Hamiltonian matrix formulation [26] to solve this problem (see Appendix B). A Bogoliubov transformation for such a case [27] brings in the magnon modes to be given by $\Omega_k = \sqrt{(ZS \pm \frac{ZS\gamma_k(\cos 2\theta_r + \Delta)}{2})^2 - (ZS\gamma_k(\cos 2\theta_r - \Delta))^2}$. The easy-planar AFM, for $h = 0$, has no preferred quantization directions in the x - y plane and hence enjoys a U(1) symmetry. Switching on the field, even infinitesimally, spontaneously breaks that symmetry, causing nondegenerate acoustic (with Goldstone excitation) and optical magnon modes to appear. Gradual increase in h reduces the gap between the modes, eventually restoring magnon degeneracy at $h = h_d = 2SZ\sqrt{(1 - \Delta)/2}$. At this point the Holstein-Primakoff transformed Hamiltonian lacks the boson hopping term between neighboring sites. We see that for the easy-axis or isotropic case, such vanishing of the hopping term occurs at $h = 0$ and magnon modes become degenerate there as well. Now also notice that for $\cos(2\theta_r) = \Delta$, Eq. (2) is devoid of the number-nonconserving

third term and the spin reference state indeed becomes the ground state. Hence we realize a factorized ground state which indicates zero quantum entanglement. This is parametrized as

$$\cos \theta_f = \sqrt{\frac{1+\Delta}{2}} \text{ and } h_f = 2ZS \cos \theta_f.$$

Similarly for the easy-axis scenario, we obtain

$$H = E_0(\theta_r) + ZS \sum_k \left[\Delta(a_k^\dagger a_k + b_k^\dagger b_k) + \gamma_k \left(\frac{\cos^2 \theta_r (1 + \Delta)}{2} (a_k^\dagger b_k + \text{H.c.}) + \frac{2 - \cos^2 \theta_r (1 + \Delta)}{2} (a_k^\dagger b_{-k}^\dagger + \text{H.c.}) \right) \right] \quad (3)$$

with $\cos \theta_r = h/SZ(1 + \Delta)$. The factorizing point is denoted by $\cos \theta_f = \sqrt{\frac{2}{1+\Delta}}$ and $h_f = ZS(1 + \Delta) \cos \theta_f$. The magnon modes are given by

$$\Omega_k = \sqrt{(\Delta SZ \pm \frac{ZS\gamma_k \cos^2 \theta_r (1+\Delta)}{2})^2 - (\frac{ZS\gamma_k (2 - \cos^2 \theta_r (1+\Delta))}{2})^2}.$$

Hence, with the application of a transverse field h , the degeneracy between the magnon modes within the reduced Brillouin zone is lost. Even at $h = 0$, nondegenerate modes are obtained as long as $\Delta < 1$. Goldstone modes are present for all values of XY anisotropy whereas the system exhibits a finite gap to lowest magnetic excitations for $\Delta > 1$.

We can understand the behavior of the magnon excitation modes intuitively from symmetry considerations. Let us first discuss the field-free XXZ model at $h = 0$. For $\Delta > 1$, spin quantization directions are along z . There is a Z_2 symmetry corresponding to the transformation $S_{i,z} \rightarrow -S_{i,z}$ (denoted by $Z_{2,z}$) as well as a U(1) symmetry corresponding to $(S_{i,x} + iS_{i,y}) = S_i^+ \rightarrow S_i^+ e^{i\phi}$ [denoted by $U_{xy}(1)$] for arbitrary angle ϕ about z . Thus the Hamiltonian possesses an overall $Z_{2,z} \otimes U_{xy}(1)$ symmetry and, consequently, two degenerate magnon modes. This remains true up to the isotropic limit when an overall SU(2) symmetry is observed in the Hamiltonian. Now a Goldstone excitation results if a continuous symmetry of the Hamiltonian is broken spontaneously by the ground state in the thermodynamic limit. The spin component along the quantization direction is a good quantum number and for $\Delta = 1$ this can be continually rotated, leaving the Hamiltonian intact and thereby yielding Goldstone modes in the spectrum. For $\Delta > 1$, the quantized component S_z does not have that liberty due to spin anisotropy and no Goldstone excitation is formed. For $\Delta < 1$, the quantization direction changes (see Fig. 1). Considering this direction to be along y (which will be the case due to spin flopping, with a transverse field along the x direction), we see that the Hamiltonian still possesses a $U_{xy}(1)$ symmetry enabling the system to have a Goldstone mode [however, note that a $U_{yz}(1)$ symmetry is not obeyed and hence only one Goldstone mode is observed in this case). The discrete $Z_{2,y}$ symmetry is obeyed. However, $U_{xz}(1)$ symmetry is lost because of the spin anisotropy of the rest of the terms: $J(S_{i,x}S_{j,x} + \Delta S_{i,z}S_{j,z})$. This, in turn, makes the magnon modes nondegenerate.

Switching on a noncommuting transverse field h results in an interesting outcome. Spin canting develops and the quantization directions (denoted by x'_A and x'_B for A and B sublattices) in the two sublattices no longer remain oppositely

directed. A magnon degeneracy, in this case, would require a $U_{y'z'}(1)$ symmetry corresponding to sublattice rotations about x' axes (by angle ϕ and $-\phi$, say, for the two sublattices, respectively). But that is absent as canting causes other phase-nonconserving terms to appear in the presence of h . So degeneracy is lifted, in general. The isotropic point at $\Delta = 1$, however, holds a sublattice symmetry corresponding to a continuous rotation of S'_x by any angle ϕ (and $-\phi$ on the other sublattice) about an axis which lies in the $x'-x$ plane. This results in the appearance of a Goldstone mode (and not two Goldstone modes because of the restriction on the axis of rotation), which survives until $h < h_c$. Beyond h_c , both x'_A and x'_B overlap with the x direction, ruling out any spontaneously broken symmetry for the ground state. Next, we see that for $h = h_d$, magnon degeneracy resurfaces for planar anisotropy. This is the singular point where coefficients of the fluctuation terms $S_i^+ S_j^-$ vanish and the Hamiltonian is invariant under a sublattice rotation by an arbitrary angle ϕ (and $-\phi$ on the other sublattice) in the $y'-z'$ plane. This reappearance of $U_{y'z'}(1)$ sublattice symmetry brings back degenerate magnon modes.

For $\Delta < 1$, the lower and higher magnon branches start moving towards each other as h is increased from zero and eventually a magnon band crossing occurs at $h = h_d$. At the critical field h_c , the magnon spectrum contains an acoustic and an optical mode. In contrast, an isotropic AFM has degenerate acoustic modes at $h = 0$ whereas an easy-axis AFM has degenerate optical modes (i.e., the minimum magnon energy is positive). In either case a finite h lifts the magnon degeneracy, resulting in the appearance of an acoustic-optical mode pair at $h = h_c$. But there is no band crossing. However, for an easy-plane AFM, we see an acoustic and an optical mode due to spontaneous breaking of the $U(1)$ symmetry at $h = 0$. With increase in h , the gap between the modes reduces and they cross each other at some intermediate field finally to become an acoustic-optical mode pair again for $h = h_c$ (but this time, the acoustic mode at $h = 0$ evolves to become an optical mode at $h = h_c$ and vice versa). This feature can be observed in neutron-scattering experiments, where the density of states shows large intensities at the field where magnon degeneracy appears. Also, by experimentally probing the lowest energy excitations, a change in the excitation spectrum can be detected during field tuning across the particular field exhibiting degeneracy.

Figure 2 demonstrates such behavior, showing the magnon dispersion plots for easy-axis $\Delta = 2$, easy-planar $\Delta = 0.5$, and isotropic $\Delta = 1$ at $k_y = 0$. The gapped and gapless nature of the Ising and XY anisotropy, respectively, can be readily seen there.

This SWT analysis (call it $\text{SWT}_a^{(1)}$) indicates a maximum field value $h = h_c$ with $h_c = 2ZS$ for $|\Delta| < 1$ and $h_c = ZS(1 + \Delta)$ for $\Delta \geq 1$, up to which this method can be meaningfully pursued as θ no longer remains real beyond that. With an increase in h , calculations eventually lead to a gapless mode at $h = h_c$ thereby indicating the limit beyond which the choice of given reference state fails. In this regard, it may also be pointed out that, with an increase in h , the spin deviation ϵ (a measure of quantum fluctuation in this case) consistently decreases to become zero at $h = h_f$.

For large h (i.e., $h \geq h_c$), $E_0(\theta)$ also becomes a minimum at $\theta = 0$ and we consider, instead, a different prescription

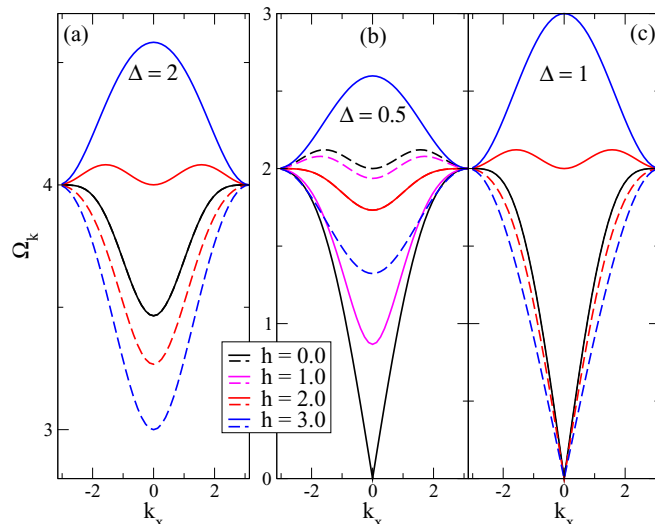


FIG. 2. Magnon modes Ω_k of the $S = 1/2$ XXZ model on the square lattice as a function of momentum k_x (with $k_y = 0$) for various values of the transverse field h and spin-exchange anisotropy (a) $\Delta = 2.0$, (b) $\Delta = 0.5$, and (c) $\Delta = 1.0$.

(call it $\text{SWT}_b^{(1)}$), with the ferromagnetic state along the x direction being the new spin reference state. The $\text{SWT}_b^{(1)}$ calculation gives the magnon dispersion expression to be $\Omega_k = \sqrt{(h - SZ + \frac{1+\Delta}{2}\gamma_k SZ)^2 - (\frac{\Delta-1}{2}\gamma_k SZ)^2}$, where the measure of the critical field for full polarization becomes $h'_c = SZ + \frac{1+\Delta}{2}SZ + \frac{|\Delta-1|}{2}SZ$ (see Appendix C). Notice that $h_c = h'_c$, as it should be. Additionally at the Heisenberg point, we obtain $h_c = h_f$ as well.

The sublattice magnetization along the rotated x directions can be obtained as $m_s = S - \epsilon$, where spin deviation $\epsilon = \frac{1}{N} \sum_k (\langle a_k^\dagger a_k \rangle + \langle b_k^\dagger b_k \rangle)$. From there the magnetization along the field direction can be obtained as $m_x = m_s \cos \theta_f$. The plots of m_x for various h are shown in Fig. 3, highlighting also the results from QMC calculations to be discussed below. Notice that the magnetization as obtained by linear spin-wave analysis and QMC calculations match exactly at $h = 0$ and h_f . At $h = 0$, the rotated quantized directions are perpendicular to the x direction, thereby ensuring that $m_x = 0$ there. On the other hand, h_f is the factorization point where we get the factorized ground state with $\epsilon = 0$ and thus magnetization becomes $m_x = S \cos \theta_f$. At the factorization field, the ground state is believed to be a direct product state, which explains the agreement between QMC simulations and $\text{SWT}_a^{(1)}$ analysis (i.e., there are no quantum corrections at h_f).

Another quantity of interest, in this reference, is the staggered magnetization m_s^\perp orthogonal to the field direction and along the spin quantization direction at zero field (infinitesimally small field, in the easy-plane case, however). For the transverse field along x , these are the z or y directions in an easy-axis or easy-plane XXZ model, respectively (see Fig. 1). Thus m_s^\perp is obtained as $m_s^\perp = m_s \sin \theta_f$. Figure 4 shows the plot of m_s^\perp as a function of transverse field h . A reduction of spin fluctuation with field (for $h < h_f$) causes m_s^\perp to increase while a spin canting towards the field direction reduces the magnetization component along the perpendicular direction.

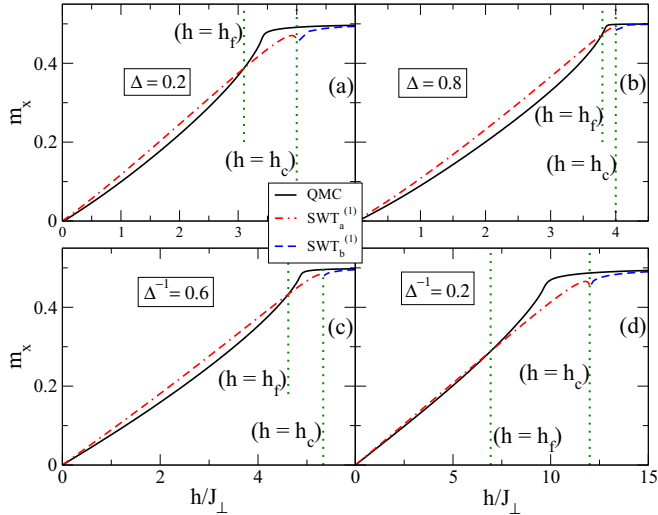


FIG. 3. Magnetization m_x along the field direction of the $S = 1/2$ XXZ model on a square lattice for (a) $\Delta = 0.2$, (b) $\Delta = 0.8$, (c) $\Delta^{-1} = 0.6$, and (d) $\Delta^{-1} = 0.2$, as a function of the transverse field h . The comparison between QMC and $\text{SWT}_a^{(1)}$, $\text{SWT}_b^{(1)}$ results is given. The locations of h_f and h_c are also shown by the dotted lines.

These two effects together determine the behavior of m_s^\perp under the variation of the field. In the easy-plane XXZ model, the former (latter) one dominates for small (large) field values and we see m_s^\perp initially increase with h , then pass through a maximum, and finally decrease down to zero at h_c (see also Ref. [15]). For large anisotropy (i.e., large Δ), however, spin fluctuations are never strong enough to cause such an initial increase in m_s^\perp for small field values.

We should also mention here that the spin deviation ϵ leaves room for correction to the spin-wave results as that is what contributes to the next higher order spin-wave expansion. At $h = 0$, ϵ decreases as we move away from the Heisenberg point. But ϵ also consistently decreases with h becoming zero at the factorization point. Beyond h_f , ϵ

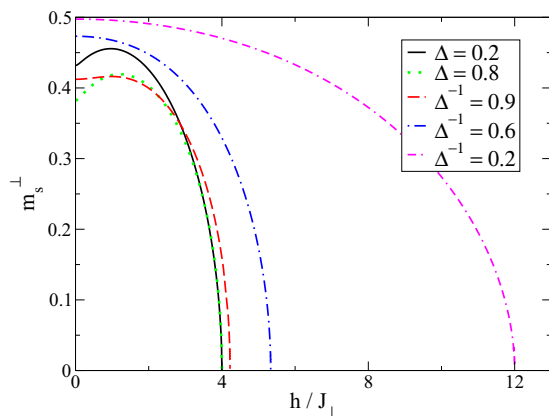


FIG. 4. Staggered magnetization m_s^\perp , orthogonal to the field direction (see Sec. III for details) in an $S = 1/2$ XXZ model on a square lattice, as a function of the transverse field h for different values of Δ .

increases again, more sharply for Δ sufficiently away from unity. This indicates the fluctuations around the quantum critical point and demonstrates the inability of mean field SWT to describe the physics precisely. That is why, in Fig. 3, the magnetization plots around h_c show some unphysical turning, already witnessed for an Ising AFM (see Ref. [28]). As the Heisenberg point has $h_c = h_f$, ϵ remains zero there and a linear SWT remains a good theory. But away from $\Delta = 1$, ϵ starts getting bigger with larger spin anisotropy, making mean-field SWT estimates more inappropriate at $h \sim h_c$. So the phase boundaries obtained using linear SWT differ more from QMC estimates in Fig. 5 for Δ farther away from unity. See that the unphysical behavior in m_x for $h \sim h_c$ also gets pronounced mostly away from $\Delta = 1$ [compare results in Figs. 3(a) and 3(d) with those of Figs. 3(b) and 3(c)].

A linear SWT (i.e., $\text{SWT}_a^{(1)}$ and $\text{SWT}_b^{(1)}$), thus, cannot predict an accurate phase boundary, as compared to the QMC calculations. However, we notice that a second-order correction to linear SWT (see Appendix D) improves the result and also give phase boundaries close to the QMC predictions [see $\text{SWT}^{(2)}$ results in Fig. 5(a)]. A perturbation analysis (see Appendix F) at the crossover point between full polarization and the one with all but one spin flipped also describes the transitions better and gives phase boundaries close to that obtained by QMC calculations.

A. Quasi-1D models

Following our calculations, magnon modes can also be obtained for the quasi-1D XXZ model. For f being the fraction of the spin-exchange interaction strength along the y direction, as compared to that along x , the magnon dispersion Ω_k is given as

$$\begin{aligned} \Delta < 1 : \Omega_k^2 &= ((1+f) \pm \gamma'_k(\cos 2\theta_r + \Delta))^2 \\ &\quad - (\gamma'_k(\cos 2\theta_r - \Delta))^2, \\ \Delta > 1 : \Omega_k^2 &= (\Delta(1+f) \pm \gamma'_k \cos^2 \theta_r (1+\Delta))^2 \\ &\quad - (\gamma'_k(2 - \cos^2 \theta_r (1+\Delta)))^2, \end{aligned} \quad (4)$$

where $\gamma'_k = [\cos(k_x) + f \cos(k_y)]/2$. This is a good estimate for elementary excitations as long as x is not very small, because deconfined spinons appear, otherwise affecting the excitation modes [29].

IV. QUANTUM MONTE CARLO

The typical way of dealing with transverse fields within the stochastic series expansion (SSE) formalism, or QMC calculations more generically, has been to treat them as adding individual raising and lowering operators to the XXZ Hamiltonian. This method has been successful in describing ferromagnetic systems, and details of this typical implementation of transverse fields can be found in Refs. [30,31]. However, this approach is not suitable for antiferromagnetic models, as the off-diagonal nature of the transverse field complicates the sublattice rotation necessary to transform the Hamiltonian into a sign-problem-free form.

In this work, we take an alternative approach by choosing the direction of the applied magnetic field as the projection axis for spin quantum number so that the magnetic field acts

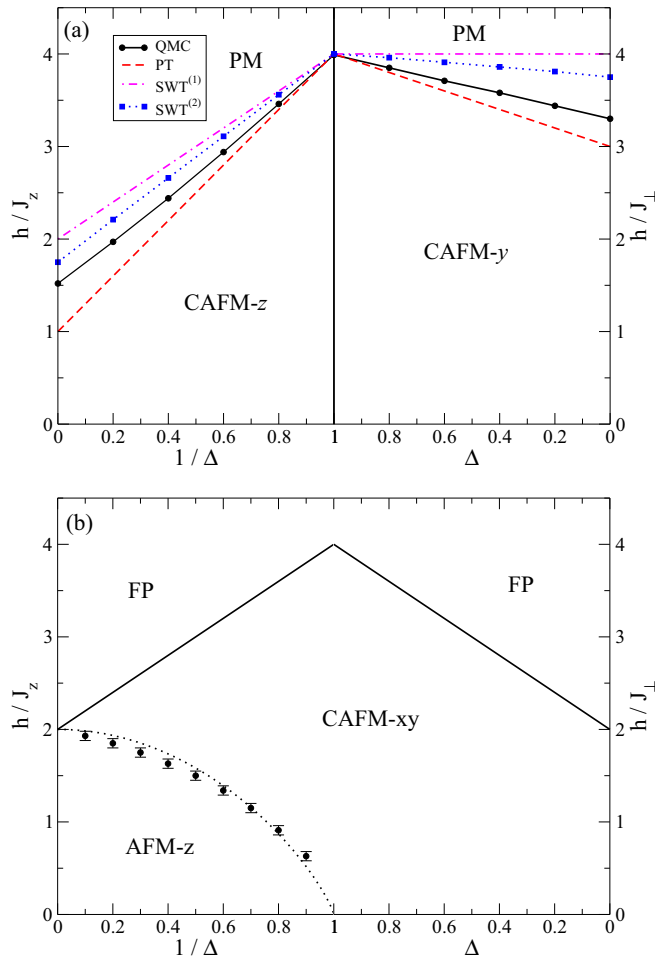


FIG. 5. Phase diagram of the $S = 1/2$ XXZ model in (a) transverse (with $\vec{h} = h\hat{x}$) and (b) longitudinal (with $\vec{h} = h\hat{z}$) magnetic fields. Within (a), phase boundaries between the canted Ising states (CAFM- z and CAFM- y) and the nearly saturated paramagnetic (PM) phase are shown for quantum Monte Carlo (QMC), first-order perturbation theory (PT), first-order spin wave theory ($SWT^{(1)}$), and second-order spin wave theory ($SWT^{(2)}$). Solid black lines represent exact boundaries by QMC. Dashed lines represent analytic results from PT (red) and $SWT^{(1)}$ (magenta) while numerical data points from QMC (black) and $SWT^{(2)}$ (blue) are shown as well. QMC data points in (a) and (b) are determined by finite-size crossings of $\rho_s L$ and energy level crossings, respectively.

upon the spins via diagonal operators (see Appendix E). The Hamiltonian for the TF-XXZ model is given by

$$\mathcal{H} = J_{\perp} \sum_{\langle ij \rangle} S_i^x S_j^x + S_i^y S_j^y + \Delta S_i^z S_j^z - h \sum_i S_i^x. \quad (5)$$

Choosing the x axis as our spin quantization axis, we rewrite the above Hamiltonian in terms of the ladder operators $S^{\pm} = S^y \pm iS^z$ to find

$$\begin{aligned} \mathcal{H} = J_{\perp} \sum_{\langle ij \rangle} S_i^x S_j^x + \frac{1-\Delta}{4} (S_i^+ S_j^+ + S_i^- S_j^-) \\ + \frac{1+\Delta}{4} (S_i^+ S_j^- + S_i^- S_j^+) - h \sum_i S_i^x. \end{aligned} \quad (6)$$

This Hamiltonian can be shown to be free of the QMC “sign problem” for bipartite lattices by choosing an appropriate (sub)lattice rotation, or by keeping track of the overall sign of the vertex weights in the operator string (for more details, see Appendix E).

In order to accommodate planar anisotropy, additional vertices need to be included compared to the standard ones required for axially anisotropic Hamiltonians. This was noted by Roscilde *et al.* in their earlier study of the TF-XXZ model [16] and has also been discussed in relation to the quantum compass model on a square lattice by Wenzel *et al.* [32,33]. Here, we comment that while the added terms $S_i^+ S_j^+$ and $S_i^- S_j^-$ break the $U(1)$ symmetry of the zero-field XXZ model, they preserve a Z_2 symmetry corresponding to the total magnetization modulo 2. This turns out to be sufficient to guarantee that link discontinuities in the directed loop update can only occur in pairs, and therefore we may use the standard directed loop equations (though they now act on 4×4 matrices of vertex weights; we use “solution B” of Syljuåsen [31]).

Using the QMC scheme described above, we have obtained the magnetic phase diagram as a function of spin-exchange anisotropy and applied magnetic field (Fig. 5). For a field along the longitudinal direction, h_z , the ground-state phase diagram is relatively simple and well known. At the isotropic point ($\Delta = 1$), in the absence of any external field the system is in a gapless Néel phase with a spontaneously chosen quantization axis. When a field is turned on, the AFM ordering is confined to the x - y plane, and a nonzero uniform magnetization is induced parallel to the applied field. We refer to this canted AFM phase as CAFM- xy . The canting increases monotonically with increasing field and the system becomes fully polarized at a saturation field, $h_s = ZS(J_{\perp} + J_z)$. Interestingly, the expression for the saturation field is an exact result. Away from the Heisenberg point, for XY-like anisotropy ($\Delta < 1$), the ground state at zero field has long-range antiferromagnetic order with spontaneously broken symmetry in the x - y plane (AFM- xy) and gapless excitations. The field-induced behavior is qualitatively similar to that in the Heisenberg limit: the ground state acquires a canting of the spins parallel to the field (CAFM- xy), which increases monotonically up to saturation. For Ising-like anisotropy ($\Delta > 1$), the ground state is characterized by longitudinal antiferromagnetic order with a finite gap to lowest spin excitations. With increasing field, the system remains in the AFM- z phase up to a critical point, at which point there is a transition to the CAFM- xy phase accompanied by the closing of the spin gap. The critical field of this first-order phase transition can be determined by an energy level crossing in the QMC data. Upon further increasing the field, the canting increases until it reaches saturation.

The situation is more complex for transverse field. As shown in Fig. 5, under a small transverse field the XXZ model displays two phases: the canted AFM- y phase (CAFM- y) and the canted AFM- z phase (CAFM- z). The CAFM- y and CAFM- z phases possess uniform magnetization along the x axis simultaneously with antiferromagnetic order along the y and z axes, respectively. The canting along the respective axes increases monotonically, but the system reaches saturation only at an infinite field strength. Instead, there is a critical field above which long-range order is lost and the system enters

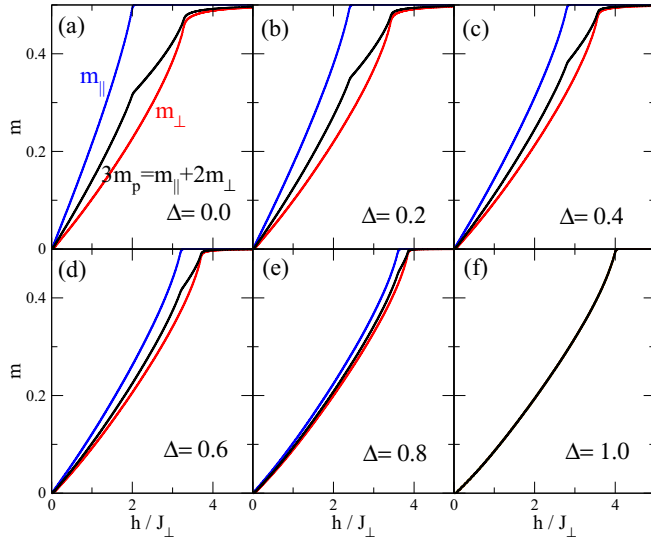


FIG. 6. Powder averages for XY-like anisotropies. Transverse field data in red, longitudinal field data in blue, and powder average in black.

a partially polarized state. Up to first order in perturbation theory (see Appendix F) the critical field is estimated as $h_c = ZS(3J_\perp + J_z)/2$. The phase transition at this critical field is continuous and belongs to the Ising universality class in $2 + 1$ dimensions [34]. This field can be accurately determined with QMC data by using finite-size scaling of the structure factor of the staggered magnetization along the y or z axis. It can be pointed out here that the mean-field SWT overestimates the critical field and thus it is, in general, higher than the values obtained using QMC data.

The powder average for magnetization is given by

$$3m_p = 2m_\perp + m_\parallel, \quad (7)$$

where m_\perp and m_\parallel are magnetizations for external magnetic field perpendicular and parallel to the easy direction (i.e., z), respectively. So $m_\parallel = m_z$ for longitudinal fields along the z direction and $m_\perp = m_x$ for transverse fields along the x direction. Within the QMC approach, these are calculated as $m_{x(z)} = \frac{1}{N} \sum_i S_{i,x(z)}$. Equation (7) can be obtained by integrating the well-known powder average formula for susceptibility [35]. In Figs. 6 and 7 we show the powder averaged magnetization (m_p) as a function of applied magnetic field for XY- and Ising-like anisotropy, respectively. Notice that the variation of m_p with field develops a kink (or jump) before the saturated field value for easy-planar (easy-axis) anisotropy when Δ is away from unity. This is also realized in magnetization measurements from powder samples with easy-planar anisotropy [22]. Furthermore, we find that a temperature variation of the powdered magnetization profile shows a gradual thermal smoothing of such kink features (see Fig. 8), in tune with the observations from polycrystalline materials [22]. The inset in Fig. 8 captures the behavior of the susceptibility $\chi = dm_p/dh$ where two peaks can be witnessed at low temperatures. These peaks are due to critical points where antiferromagnetic order ceases: the first in response to the longitudinal component of the field and the second in response to the transverse component of field. For easy-planar

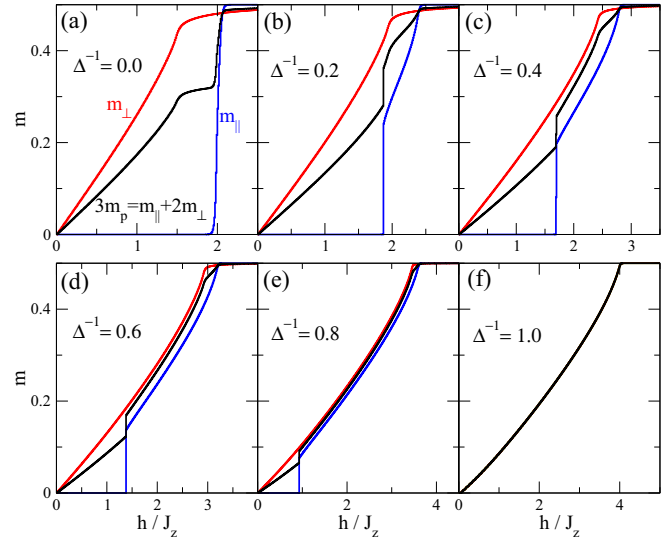


FIG. 7. Powder averages for Ising-like anisotropies. Transverse field data in red, longitudinal field data in blue, and powder average in black.

anisotropy, peaks of comparable height are obtained as also observed experimentally and reported in Ref. [22]. For easy-axis anisotropy, on the other hand, the first peak is a sharp one due to the sudden increase in magnetization occurring at the spin-flop transition for the longitudinal component of the field. All these observations indicate that an analytic calculation followed by numerical computations of thermalized states in the presence of longitudinal and transverse fields contributes significantly in understanding the magnetic response from powder samples.

V. DISCUSSION

We have studied the ground-state phases and low-lying excitations of the two-dimensional XXZ model—with both

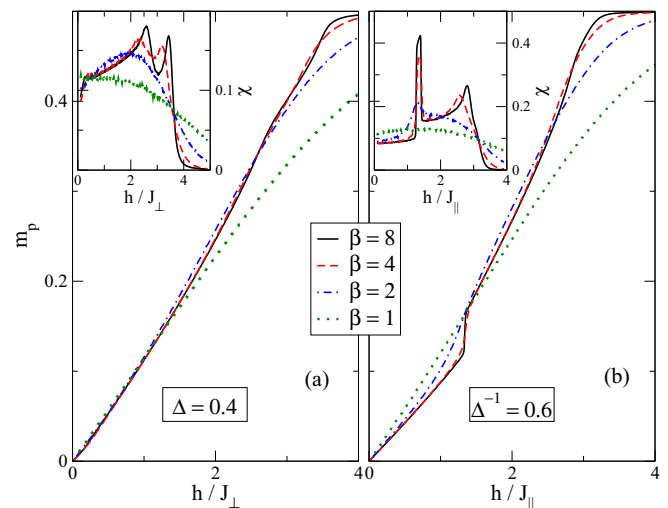


FIG. 8. Powder averages m_p vs field h for (a) easy-planar $\Delta = 0.4$ and (b) easy-axis $\Delta^{-1} = 0.6$ cases at different temperatures. Here $\beta = 1/k_B T$ values are in units of (a) J_\perp or (b) J_\parallel . The inset shows the corresponding susceptibilities.

Ising-like and XY-like exchange anisotropies—in the presence of a transverse magnetic field. The transverse field causes a tilting of the sublattice magnetization, producing canted magnetic orders in the system. For a small field, the overall magnetization grows slowly as the field competes with the spin anisotropy. Both the longitudinal and transverse components of the magnetization are probed, as is the low-lying excitation spectrum. The evolution of the magnon excitation with increasing field is examined in detail using spin-wave theory, with particular emphasis on the nature of the excitation spectrum at the entanglement free point. For this critical value of the field, quantum fluctuations are suppressed, resulting in an unentangled ground state at a finite field value. Beyond this point, however, fluctuation shoots up fast to become a maximum at the transition point h_c . The spin-wave results are complemented by and benchmarked against large-scale QMC simulations, yielding a deeper understanding of the magnetic properties across a wide range of Hamiltonian parameters. We find that in a longitudinal field, the saturation field can be calculated exactly to be $h_s = ZS(J_\perp + J_z)$. In a transverse field, on the contrary, the expression is no longer exact, in part because the saturation field is replaced by a critical field. Up

to first order in perturbation theory the critical field is given by $h_c = ZS(3J_\perp + J_z)/2$. We also provide an estimate of magnon excitation modes in quasi-1D antiferromagnets. Finally, we use our QMC results to calculate the weighted average of the longitudinal and transverse components of the magnetization as an estimate of powder averaged neutron-scattering data in polycrystalline samples. This will be useful in analyzing experimental results in quantum magnets where large single crystals are not available.

ACKNOWLEDGMENTS

S.K. thanks K. Sengupta for useful discussions. Financial support from CSIR, India, under Scientists' Pool Scheme No. 13(8764-A)/2015-Pool (SK) and from the Ministry of Education, Singapore, through Grant No. MOE2014-T2-1-112 (PS) is gratefully acknowledged.

APPENDIX A: DETAILS OF SWT⁽¹⁾

When we write the Hamiltonian for $\Delta < 1$ in terms of the sublattice rotations, we obtain

$$H = \sum_{(ij)} H_{ij} = \sum_{(ij)} \left[\Delta S_i^z S_j^z + \cos(2\theta)(S_i^x S_j^x + S_i^y S_j^y) + \sin(2\theta)(S_i^x S_j^y - S_i^y S_j^x) - \frac{h}{Z} \left((S_i^x + S_j^x) \cos \theta - (S_i^y - S_j^y) \sin \theta \right) \right]. \quad (\text{A1})$$

Here the Hamiltonian is written in units of J_{xy} . With x being the quantization axis and $S_i^\pm = S_i^y \pm iS_i^z$ the raising and lowering operators, we can rewrite the Hamiltonian as

$$H = \sum_{(ij)} \left[\cos(2\theta) S_i^x S_j^x - \frac{h}{Z} (S_i^x + S_j^x) \cos \theta + \frac{\cos 2\theta}{4} (S_i^+ + S_i^-)(S_j^+ + S_j^-) - \frac{\Delta}{4} (S_i^+ - S_i^-)(S_j^+ - S_j^-) + \sin 2\theta \left((S - n_i) \frac{S_j^+ + S_j^-}{2} - (S - n_j) \frac{S_i^+ + S_i^-}{2} \right) + \frac{h}{Z} \left(\frac{S_i^+ + S_i^-}{2} - \frac{S_j^+ + S_j^-}{2} \right) \sin \theta \right]. \quad (\text{A2})$$

Now applying the Holstein-Primakoff transformation for SWT in a ferromagnet, we get $S_i^x = S - a_i^\dagger a_i = S - n_i$ ($S_j^x = S - b_j^\dagger b_j = S - n_j$) and $S_i^+ = \sqrt{2S} a_i$ ($S_j^+ = \sqrt{2S} b_j$), where i (j) denotes the \uparrow (\downarrow) sublattice along x , and a_i 's (b_j 's) are the bosonic operators in the \uparrow (\downarrow) sublattice. Hence we obtain

$$H = \sum_{(ij)} \left[\cos(2\theta)(S - n_i)(S - n_j) - \frac{h}{Z} (2S - n_i - n_j) \cos \theta + \frac{\cos 2\theta - \Delta}{4} (a_i^\dagger b_j^\dagger + \text{H.c.}) + \frac{\cos 2\theta + \Delta}{4} (a_i^\dagger b_j + \text{H.c.}) + \frac{2h \sin \theta / Z - \sin 2\theta}{4} (a_i^\dagger - b_j^\dagger + \text{H.c.}) \right] \\ = E_0(\theta) + \sum_{(ij)} \left[-\cos(2\theta)S(n_i + n_j) + \frac{h}{Z} (n_i + n_j) \cos \theta + \frac{\cos 2\theta - \Delta}{4} (a_i^\dagger b_j^\dagger + \text{H.c.}) + \frac{\cos 2\theta + \Delta}{4} (a_i^\dagger b_j + \text{H.c.}) + \frac{2h \sin \theta / Z - \sin 2\theta}{4} (a_i^\dagger - b_j^\dagger + \text{H.c.}) \right]. \quad (\text{A3})$$

By minimizing $E_0(\theta)$, we obtain the reference angle θ_r as $\cos \theta_r = h/2ZS$. Thus we fix the reference state for spin-wave expansion. A consecutive Fourier transformation, thereafter, leads to

$$H = E_0(\theta_r) + \sum_k \left[\frac{Z}{2} (a_k^\dagger a_k + b_k^\dagger b_k) + Z\gamma_k \left(\frac{\cos 2\theta_r + \Delta}{4} (a_k^\dagger b_k + \text{H.c.}) + \frac{\cos 2\theta_r - \Delta}{4} (a_k^\dagger b_{-k}^\dagger + \text{H.c.}) \right) \right]. \quad (\text{A4})$$

Finally a Bogoliubov transformation brings in the magnon modes to be given by $\Omega_k = \sqrt{(\frac{Z}{2} \pm \frac{Z\gamma_k(\cos 2\theta_r + \Delta)}{4})^2 - (\frac{Z\gamma_k(\cos 2\theta_r - \Delta)}{4})^2}$. Notice that for $\cos(2\theta_r) = \Delta$, the Hamiltonian (A4) becomes diagonal, making the reference state there the actual factorized ground state. So at the factorization point, $\cos \theta_f = \sqrt{\frac{1+\Delta}{2}}$ and $h_f = 2ZS \cos \theta_f$.

Now for $\Delta > 1$, we have

$$H = \sum_{(ij)} \left[S_i^x S_j^x (\cos^2 \theta - \Delta \sin^2 \theta) + \frac{(S_i^+ + S_i^-)(S_j^+ + S_j^-)}{4} + \frac{\sin(2\theta)(1 + \Delta)}{4i} (S_i^x (S_j^+ - S_j^-) - (S_i^+ - S_i^-) S_j^x) - \frac{(S_i^+ - S_i^-)(S_j^+ - S_j^-)}{4} (-\sin^2 \theta + \Delta \cos^2 \theta) - \frac{h}{Z} \left((S_i^x + S_j^x) \cos \theta - \frac{(S_i^+ - S_i^-) - (S_j^+ - S_j^-)}{2i} \sin \theta \right) \right], \quad (\text{A5})$$

within linear spin-wave theory, which becomes

$$H = E_0(\theta) + \sum_{(ij)} \left[(\Delta \sin^2 \theta - \cos^2 \theta) S(n_i + n_j) + \frac{h}{Z} (n_i + n_j) \cos \theta + \frac{1 + \sin^2 \theta - \Delta \cos^2 \theta}{4} (a_i^\dagger b_j^\dagger + \text{H.c.}) + \frac{1 - \sin^2 \theta + \Delta \cos^2 \theta}{4} (a_i^\dagger b_j + \text{H.c.}) + \left(\frac{h \sin \theta}{2Zi} - \frac{\sin(2\theta)(1 + \Delta)}{4i} \right) (a_i^\dagger - b_j^\dagger - \text{H.c.}) \right].$$

Minimizing $E_0(\theta)$ gives $\cos \theta_r = h/SZ(1 + \Delta)$. And with this and by Fourier transformation we obtain

$$H = E_0(\theta_r) + Z \sum_k \left[\frac{\Delta}{2} (a_k^\dagger a_k + b_k^\dagger b_k) + \gamma_k \left(\frac{\cos^2 \theta_r (1 + \Delta)}{4} (a_k^\dagger b_k + \text{H.c.}) + \frac{2 - \cos^2 \theta_r (1 + \Delta)}{4} (a_k^\dagger b_{-k}^\dagger + \text{H.c.}) \right) \right], \quad (\text{A6})$$

with $\cos \theta_r = h/SZ(1 + \Delta)$. The factorizing point is denoted by $\cos \theta_f = \sqrt{\frac{2}{1+\Delta}}$ and $h_f = ZS(1 + \Delta) \cos \theta_f$. The magnon modes are given by $\Omega_k = \sqrt{(\frac{\Delta Z}{2} \pm \frac{Z\gamma_k \cos^2 \theta_r (1 + \Delta)}{4})^2 - (\frac{Z\gamma_k (2 - \cos^2 \theta_r (1 + \Delta))}{4})^2}$.

APPENDIX B: OBTAINING MAGNON MODES FROM A 4×4 SPIN-WAVE HAMILTONIAN

Let us now construct the magnon modes from the k -space Hamiltonian,

$$H = E_0 + \sum_k [A_k (a_k^\dagger a_k + b_k^\dagger b_k) + (B_k a_k^\dagger b_k + C_k a_k^\dagger b_{-k}^\dagger + \text{H.c.})]. \quad (\text{B1})$$

We can write this as $H = E_0 + \sum_k \langle \phi_k | H_k | \phi_k \rangle$, where $|\phi_k\rangle = (a_k, b_{-k}^\dagger, b_k, a_{-k}^\dagger)^T$ and

$$H_k = \begin{pmatrix} A_k & C_k & B_k & 0 \\ C_k & A_k & 0 & B_k \\ B_k & 0 & A_k & C_k \\ 0 & B_k & C_k & A_k \end{pmatrix}.$$

From there we can obtain the diagonalized version as outlined in Refs. [26,27]. A Bogoliubov transformation brings in the states $|\psi_k\rangle = U|\phi_k\rangle$, where $|\psi_k\rangle = (\alpha_k, \beta_{-k}^\dagger, \beta_k, \alpha_{-k}^\dagger)^T$ and U is a coefficient matrix so that $U^\dagger H_k U$ becomes a diagonal matrix with eigenvalues λ_k 's. This as well as the bosonization of the new variables α_k and β_k requires $\text{Det}[M_k] = 0$ for a certain matrix M_k , given as

$$M_k = \begin{pmatrix} A_k - \lambda_k & C_k & B_k & 0 \\ C_k & A_k + \lambda_k & 0 & B_k \\ B_k & 0 & A_k - \lambda_k & C_k \\ 0 & B_k & C_k & A_k + \lambda_k \end{pmatrix}.$$

Hence we get $\lambda_{k(\pm)} = [(A_k \pm B_k)^2 - C_k^2]^{0.5}$ and the Hamiltonian becomes

$$H = E'_0 + \sum_k [\lambda_{k(+)} \alpha_k^\dagger \alpha_k + \lambda_{k(-)} \beta_k^\dagger \beta_k]. \quad (\text{B2})$$

Solving for the coefficient matrix U (see Ref. [27]), we can also obtain the spin deviation given as $\epsilon = \frac{1}{N} \sum_k (\langle a_k^\dagger a_k \rangle + \langle b_k^\dagger b_k \rangle)$, where $\langle \dots \rangle$ denotes the ground-state average.

APPENDIX C: DETAILS OF SWT⁽¹⁾

On the other hand, if we want to do the spin-wave analysis for large h values we rather consider the ferromagnetic spin orientations along the field direction x to be the quantization axis and take that ferromagnetic state (with no sublattice division) to be the spin reference state. A $\pi/2$ rotation about the y axis moves the z axis to the field direction and that becomes the z axis in the transformed coordinates. Within such definition, the transverse field XXZ Hamiltonian becomes

$$H = \sum_{(ij)} \left[S_i^z S_j^z + \frac{\Delta - 1}{4} (S_i^+ S_j^+ + \text{H.c.}) + \frac{1 + \Delta}{4} (S_i^+ S_j^- + \text{H.c.}) \right] - h \sum_i S_i^z. \quad (\text{C1})$$

Using linear spin-wave theory, this becomes

$$H = E_0 + (h - SZ) \sum_i n_i + \sum_{(ij)} \left(\frac{1 + \Delta}{4} a_i^\dagger a_j + \frac{\Delta - 1}{4} a_i^\dagger a_j^\dagger + \text{H.c.} \right). \quad (\text{C2})$$

Then we do the Fourier transformation to get

$$H = E_0 + (h - SZ) \sum_k n_k + \sum_k \left[\frac{1 + \Delta}{2} \gamma_k SZ a_k^\dagger a_k + \frac{\Delta - 1}{2} \gamma_k SZ (a_k a_{-k} + \text{H.c.}) \right]. \quad (\text{C3})$$

Finally a Bogoliubov transformation gives

$$H = E'_0 + \sum_k \Omega_k \tilde{a}_k^\dagger \tilde{a}_k, \quad (\text{C4})$$

where $\Omega_k = \sqrt{(h - SZ + \frac{1+\Delta}{2} \gamma_k SZ)^2 - (\frac{\Delta-1}{2} \gamma_k SZ)^2}$. So this gives the critical h to be $h'_c = SZ + \frac{1+\Delta}{2} SZ + \frac{|\Delta-1|}{2} SZ$.

APPENDIX D: SECOND-ORDER SPIN-WAVE THEORY AT LARGE FIELDS

In order to do a second-order correction to the linear SWT_b⁽¹⁾ at high fields, we see that the higher-order correction to spin-wave expansion, for a ferromagnetic reference state, gives us a modified $S_i^+ = \sqrt{2S}(a_i - \frac{n_i a_i}{2})$. This alters the off-site interaction terms as

$$\begin{aligned} S_i^+ S_j^- &= a_i a_j^\dagger \left(1 - \frac{n_j}{2}\right) - \frac{n_i a_i a_j^\dagger}{2}, \\ S_i^+ S_j^+ &= a_i a_j \left(1 - \frac{n_j}{2}\right) - \frac{n_i a_i a_j}{2}, \end{aligned} \quad (\text{D1})$$

up to the quartic order of the bosonic operators. A mean-field treatment for a product of variables A and B can be given as $AB = \overline{A}\overline{B} + \overline{A}B$, where \overline{A} and \overline{B} are the respective averages. Applying that to the quartic correction terms, we obtain the modified magnon mode expressions of SWT_b⁽¹⁾ to be

$$\begin{aligned} \Omega_k &= \sqrt{A_{1k}^2 - A_{2k}^2}, \\ \text{where } A_{1k} &= h - SZ \left[1 - \frac{1 + \Delta}{2} \{\gamma_k(1 - \epsilon) - \delta\} + (\Delta - 1)\eta \right], \\ A_{2k} &= \frac{\Delta - 1}{2} \gamma_k SZ(1 - \epsilon). \end{aligned} \quad (\text{D2})$$

The critical field becomes

$$\begin{aligned} h_c^{(2)} &= SZ \left[1 + \frac{1 + \Delta}{2} (1 - \epsilon - \delta) - (\Delta - 1)\eta + \frac{|\Delta - 1|}{2} (1 - \epsilon) \right]. \end{aligned} \quad (\text{D3})$$

Here $\langle \overline{n_i} \rangle = \langle \overline{n_j} \rangle = \epsilon$ is the spin deviation. The other fluctuation measures $\delta = \langle a_i^\dagger a_j \rangle = \sum_k \gamma_k a_k^\dagger a_k / N$ and $\eta = \langle \overline{a_i a_j} \rangle = \sum_k \gamma_k a_k a_{-k} / N$ (see Ref. [36]). So we need to calculate both Ω_k and h_c numerically in a self-consistent manner. We obtain the critical fields at Ising and XY limits to be $h_c^{(2)}|_{\text{Ising}} = 1.75$ and $h_c^{(2)}|_{\text{XY}} = 3.75$. See that for the isotropic point $\Delta = 1$, $h'_c = 2Zs = 4$ is the factorization point where $\epsilon = 0$. Other

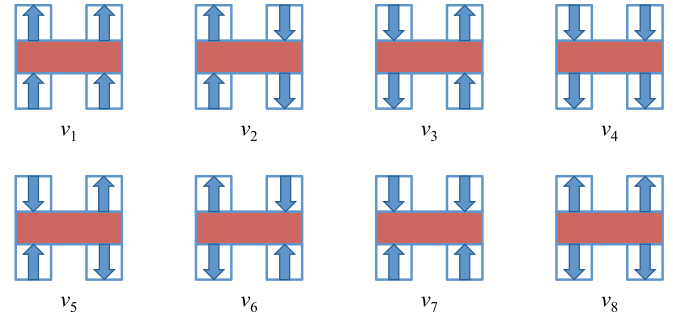


FIG. 9. The allowed diagonal ($v_1 - v_4$) and off-diagonal (v_5 and v_6) vertices for the TF-XXZ model. The first six vertices also appear in the longitudinal field XXZ model, while the last two vertices appear whenever $\Delta \neq 1$.

fluctuations δ and η are also zero at this point, which have been checked numerically.

APPENDIX E: DETAILS OF QUANTUM MONTE CARLO METHOD

In Fig. 9 we show the allowed vertices for the TF-XXZ model. This includes the addition of two number-nonconserving vertices (v_7 and v_8) to the usual six vertices ($v_1 - v_6$) of the XXZ model. On a bipartite lattice, it can be shown that the vertices v_5 and v_6 must occur an even number of times ($n_{v_5} + n_{v_6}$ is even), which is sufficient to ensure that the overall contribution to the weight function in the *diagonal sector* is positive definite. Similarly, the vertices v_7 and v_8 must also occur an even number of times ($n_{v_7} + n_{v_8}$ is even), even on nonbipartite lattices.

Measurements in the *off-diagonal sector* are also possible, but the total weight is no longer guaranteed to be positive definite. However, since the partition function is still defined in the diagonal sector, the total weight in the off-diagonal sector can be obtained by working with the absolute weights while keeping track of the overall sign of the vertex weights. Observables such as the Green's function are then calculated as the signed average over configurations. In short, measurements in the off-diagonal sector are easily obtained by using the absolute value of all off-diagonal vertex weights, while separately keeping track of the overall sign of the operator string as it evolves during the loop update. We find this method to be much simpler in practice than the standard alternative: first define a formal (sub)lattice transformation such that all off-diagonal terms become negative definite, then determine the momentum shift required to map between the original and transformed Hamiltonian observables. For the XXZ model in a longitudinal field, this becomes a sublattice rotation of π around the z axis, with a (π, π) momentum shift. In the present case, an additional lattice rotation by $\pi/2$ is required whenever $\Delta > 1$, which becomes tedious to keep track of compared to the relative simplicity of our explicit sign tracking described above. Another benefit to our method of sign tracking is that if the overall sign is ever negative at the close of the loop update, then we know that the model has a QMC sign problem. Thus, we have explicitly checked our assumption that no sign problem exists for the TF-XXZ model as defined in this paper.

APPENDIX F: DETAILS OF PERTURBATION THEORY

Let us begin by writing the unperturbed Hamiltonian as

$$\mathcal{H}_0 = J_{\perp} \sum_{\langle ij \rangle} S_i^x S_j^x - h \sum_i S_i^x, \quad (\text{F1})$$

so that the perturbed Hamiltonian becomes

$$\begin{aligned} \mathcal{H}' = & J_{\perp} \sum_{\langle ij \rangle} \frac{1-\Delta}{4} (S_i^+ S_j^+ + S_i^- S_j^-) \\ & + \frac{1+\Delta}{4} (S_i^+ S_j^- + S_i^- S_j^+). \end{aligned} \quad (\text{F2})$$

Next, we consider the zero-order (unperturbed) contribution to the energy of a state with all and all but one of its spins aligned with the magnetic field and label these energies $E_0(N \uparrow, 0 \downarrow)$

and $E_0(N-1 \uparrow, 1 \downarrow)$, respectively. It is easy to show that

$$\begin{aligned} E_0(N \uparrow, 0 \downarrow) &= \frac{NZ}{2} J_{\perp} S^2 - NBS, \\ E_0(N-1 \uparrow, 1 \downarrow) &= \left(\frac{NZ}{2} - 2Z \right) J_{\perp} S^2 - (N-2)BS. \end{aligned} \quad (\text{F3})$$

The first-order corrections can be obtained as $\langle \psi_0 | \mathcal{H}' | \psi_0 \rangle$ and are given by

$$\begin{aligned} E_1(N \uparrow, 0 \downarrow) &= 0 \\ E_1(N-1 \uparrow, 1 \downarrow) &= -Z \frac{J_{\perp} + J_z}{4}. \end{aligned} \quad (\text{F4})$$

Finally, by equating these energies up to first order (i.e., $E_0 + E_1$) we find an estimate of the critical field, where the fully saturated unperturbed state is favorable to the state with a flipped spin: $h_c = Z(3J_{\perp} + J_z)/4$.

-
- [1] S. Sachdev, *Nat. Phys.* **4**, 173 (2008).
[2] V. Zapf, M. Jaime, and C. D. Batista, *Rev. Mod. Phys.* **86**, 563 (2014).
[3] L. Balents, *Nature (London)* **464**, 199 (2010).
[4] A. W. Sandvik, *Phys. Rev. Lett.* **98**, 227202 (2007).
[5] K. Matan, T. Ono, Y. Fukumoto, T. J. Sato, J. Yamaura, M. Yano, K. Morita, and H. Tanaka, *Nat. Phys.* **6**, 865 (2010).
[6] S. A. Owerre, [arXiv:1609.03563](https://arxiv.org/abs/1609.03563); *Europhys. Lett.* **117**, 37006 (2017).
[7] J. Zhou, Q.-F. Liang, H. Weng, Y. B. Chen, S.-H. Yao, Y.-F. Chen, J. Dong, and G.-Y. Guo, *Phys. Rev. Lett.* **116**, 256601 (2016).
[8] H. Kageyama, K. Yoshimura, R. Stern, N. V. Mushnikov, K. Onizuka, M. Kato, K. Kosuge, C. P. Slichter, T. Goto, and Y. Ueda, *Phys. Rev. Lett.* **82**, 3168 (1999).
[9] O. Breunig, M. Garst, E. Sela, B. Buldmann, P. Becker, L. Bohatý, R. Müller, and T. Lorenz, *Phys. Rev. Lett.* **111**, 187202 (2013).
[10] O. Breunig, M. Garst, A. Rosch, E. Sela, B. Buldmann, P. Becker, L. Bohatý, R. Müller, and T. Lorenz, *Phys. Rev. B* **91**, 024423 (2015).
[11] M. Kenzelmann, R. Coldea, D. A. Tennant, D. Visser, M. Hofmann, P. Smeibidl, and Z. Tylczynski, *Phys. Rev. B* **65**, 144432 (2002).
[12] A. Cuccoli, T. Roscilde, V. Tognetti, R. Vaia, and P. Verrucchi, *Phys. Rev. B* **67**, 104414 (2003).
[13] M. Holschneider, W. Selke, and R. Leidl, *Phys. Rev. B* **72**, 064443 (2005).
[14] S. Yunoki, *Phys. Rev. B* **65**, 092402 (2002).
[15] P. J. Jensen, K. H. Bennemann, D. K. Morr, and H. Dreyssé, *Phys. Rev. B* **73**, 144405 (2006).
[16] T. Roscilde, P. Verrucchi, A. Fubini, S. Haas, and V. Tognetti, *Phys. Rev. Lett.* **93**, 167203 (2004); **94**, 147208 (2005).
[17] J. Abouie, A. Langari, and M. Siahatgar, *J. Phys.: Condens. Matter* **22**, 216008 (2010).
[18] H. Moradmard, M. Shahri Naseri, and S. Mahdaviyar, *J. Supercond. Novel Magn.* **27**, 1265 (2014).
[19] L. Amico, R. Fazio, A. Osterloh, and V. Vedral, *Rev. Mod. Phys.* **80**, 517 (2008).
[20] J. Kurmann, H. Thomas, and G. Müller, *Physica A (Amsterdam, Neth.)* **112**, 235 (1982).
[21] L. Amico, F. Baroni, A. Fubini, D. Patanè, V. Tognetti, and P. Verrucchi, *Phys. Rev. A* **74**, 022322 (2006).
[22] J. Brambleby, P. A. Goddard, R. D. Johnson, J. Liu, D. Kaminski, A. Ardavan, A. J. Steele, S. J. Blundell, T. Lancaster, P. Manuel, P. J. Baker, J. Singleton, S. G. Schwalbe, P. M. Spurgeon, H. E. Tran, P. K. Peterson, J. F. Corbey, and J. L. Manson, *Phys. Rev. B* **92**, 134406 (2015).
[23] M. Oshikawa and I. Affleck, *Phys. Rev. Lett.* **79**, 2883 (1997).
[24] F. H. L. Eßler, *Phys. Rev. B* **59**, 14376 (1999).
[25] S. A. Zvyagin, E. Čížmár, M. Ozerov, J. Wosnitza, R. Feyerherm, S. R. Manmana, and F. Mila, *Phys. Rev. B* **83**, 060409(R) (2011).
[26] E. Manousakis, *Phys. Rev. B* **79**, 220509(R) (2009).
[27] S. Kar, *J. Magn. Magn. Mater.* **393**, 357 (2015).
[28] L.-P. Henry, P. C. W. Holdsworth, F. Mila, and T. Roscilde, *Phys. Rev. B* **85**, 134427 (2012).
[29] A. A. Nersesyan and A. M. Tsvelik, *Phys. Rev. B* **67**, 024422 (2003).
[30] P. Henelius, A. W. Sandvik, C. Timm, and S. M. Girvin, *Phys. Rev. B* **61**, 364 (2000); P. Henelius, P. Fröbrich, P. J. Kuntz, C. Timm, and P. J. Jensen, *ibid.* **66**, 094407 (2002).
[31] O. F. Syljuåsen, *Phys. Rev. E* **67**, 046701 (2003).
[32] S. Wenzel and W. Janke, *Phys. Rev. B* **78**, 064402 (2008).
[33] S. Wenzel, W. Janke, and A. M. Läuchli, *Phys. Rev. E* **81**, 066702 (2010).
[34] A. Pelissetto and E. Vicari, *Phys. Rep.* **368**, 549 (2002).
[35] M. Rigol and R. R. P. Singh, *Phys. Rev. B* **76**, 184403 (2007).
[36] T. Coletta, N. Laflorencie, and F. Mila, *Phys. Rev. B* **85**, 104421 (2012).